

In either model, the apparent sequence specificity of some metazoan replication origins would result from modulation by the nuclear context of a primarily nonsequence-specific initiation mechanism. Indeed, *Xenopus* egg extracts are able to initiate DNA replication specifically within the Chinese hamster DHFR initiation zone if intact G<sub>1</sub>-phase nuclei are used as the substrate (28). This finding was suggested to result from nuclear structure rather than transcription, although it remains to be demonstrated that *Xenopus* egg extracts do not carry out transcription in these experiments.

The confinement of replication initiation outside of genes may have had different evolutionary consequences in organisms with different ways of life (1, 12). Protozoa and viruses with small genomes, little intergenic DNA, and requirements for rapid growth could have been favored by the emergence of efficient, sequence-specific replication origins. On the contrary, a nonsequence-specific initiation mechanism may adapt with greater flexibility to the variety of proliferation rates and nuclear contexts found in a metazoan organism.

#### REFERENCES AND NOTES

- B. J. Brewer, *Curr. Opin. Genet. Dev.* **4**, 196 (1994).
- J. L. Hamlin and P. A. Dijkwel, *ibid.* **5**, 153 (1995).
- J. P. Vaughn, P. A. Dijkwel, J. L. Hamlin, *Cell* **61**, 1075 (1990); P. A. Dijkwel and J. L. Hamlin, *Mol. Cell. Biol.* **15**, 3023 (1995).
- W. C. Burhans, L. T. Vassilev, M. S. Caddle, N. H. Heintz, M. L. DePamphilis, *Cell* **62**, 955 (1990).
- D. Kitsberg, S. Selig, I. Keshet, H. Cedar, *Nature* **366**, 588 (1993).
- M. Bénard, C. Lagnel, G. Pierron, *Nucleic Acids Res.* **23**, 1447 (1995).
- P. Hernandez, L. Martin-Parras, M. L. Martinez-Robles, J. B. Schwartzman, *EMBO J.* **12**, 1475 (1993).
- B. J. Brewer and W. L. Fangman, *Cell* **55**, 637 (1988).
- M. H. K. Linskens and J. A. Huberman, *Mol. Cell. Biol.* **8**, 4927 (1988).
- R. D. Little, T. H. K. Platt, C. Schildkraudt, *ibid.* **13**, 6600 (1993).
- B. Wiesendanger, R. Lucchini, T. Koller, J. Sogo, *Nucleic Acids Res.* **22**, 5038 (1994).
- O. Hyrien and M. Méchali, *EMBO J.* **12**, 4511 (1993).
- \_\_\_\_\_, *Nucleic Acids Res.* **20**, 1463 (1992).
- H. M. Mahbubani, T. Paull, J. K. Elder, J. J. Blow, *ibid.*, p. 1457.
- K. Shiokawa, Y. Misumi, K. Yamana, *Dev. Growth Differ.* **23**, 579 (1981).
- B. J. Brewer and W. L. Fangman, *Cell* **51**, 463 (1987).
- The frequencies of initiation ( $F_i$ ) or termination ( $F_t$ ) (number of events per kilobase pair of DNA sequence within each fragment) are here defined as

$$F_i = 1/n[1 + (2/9)(Y/O)] \quad (1)$$

$$F_t = 1/n[1 + (5/18)(Y/H)] \quad (2)$$

where  $n$  is the size of the fragment analyzed, and O, H, and Y are the percentages of bubbles, double forks, and simple forks, respectively. These formulas were derived assuming random initiation and termination and constant fork speed within the fragment (12). If initiation and termination occur with different efficiencies along the DNA sequences, these formulas tend to underestimate the actual differences between fragments (calculations not shown). Therefore, they remain valid approximations for the present study. Results from identical experiments (Table 1) varied by less than  $\pm 9\%$  for termination frequency but up to  $\pm 30\%$  for the lowest initiation

frequencies. Only much larger changes over development are discussed here. When, due to size polymorphism, Y's of larger fragments overlapped with H's of smaller fragments, we corrected the respective signals by subtracting from Y's and adding to H's the contribution of H's to the zone of overlap. This value was estimated from the area of the overlap zone and from the average signal in immediately adjacent H's free of Y's.

- M. H. K. Linskens and J. A. Huberman, *Nucleic Acids Res.* **18**, 647 (1988).
- H. G. Callan, *Proc. R. Soc. London Ser. B* **181**, 19 (1972).
- Y. Yoon, J. A. Sanchez, C. Brun, J. A. Huberman, *Mol. Cell. Biol.* **15**, 2482 (1995); P. A. Dijkwel, J. P. Vaughn, J. L. Hamlin, *Nucleic Acids Res.* **22**, 4989 (1994).
- R. Lucchini and J. M. Sogo, *Mol. Cell. Biol.* **12**, 4288 (1992).
- O. Hyrien, C. Maric, M. Mechali, data not shown; but see figure 4D in (12).
- S. B. Haase, S. S. Heinzl, M. P. Calos, *Mol. Cell. Biol.* **14**, 2516 (1994); W.-J. Pan, R. C. Gallagher, E. H. Blackburn, *ibid.* **15**, 3372 (1995); M. Snyder, R. J.

Sapolsky, R. W. Davis, *ibid.* **8**, 2184 (1988).

- R. F. J. De Winter and T. Moss, *Nucleic Acids Res.* **14**, 6041 (1986); P. Labhart and R. H. Reeder, *Cell* **45**, 431 (1986).
- C. Wu, M. Zannis-Hadjopoulos, G. B. Price, *Biochim. Biophys. Acta* **1174**, 258 (1993); E. S. Tasheva and D. J. Roufa, *Mol. Cell. Biol.* **14**, 5628 (1994); R. E. Kelly, M. L. DeRose, B. W. Draper, G. M. Wahl, *ibid.* **15**, 4136 (1995).
- R. H. Reeder, *Trends Genet.* **6**, 390 (1990).
- M. L. DePamphilis, *Trends Cell Biol.* **3**, 161 (1993).
- D. M. Gilbert, H. Miyazawa, M. L. DePamphilis, *Mol. Cell. Biol.* **15**, 2942 (1995).
- P. A. Dijkwel, J. P. Vaughn, J. L. Hamlin, *ibid.* **11**, 3850 (1991).
- We thank S. Bocquet for help with embryo collection and P. Brooks, G. Pierron, Y. Vassetsky, and P. Hughes for critical reading of the manuscript. Supported by grants from INSERM, the Association pour la Recherche sur le Cancer, the European Community, and the Ligue Nationale Française contre le Cancer.

2 May 1995; accepted 19 September 1995

## A Left-Handed Parallel $\beta$ Helix in the Structure of UDP-N-Acetylglucosamine Acyltransferase

Christian R. H. Raetz and Steven L. Roderick\*

UDP-N-acetylglucosamine 3-O-acyltransferase (LpxA) catalyzes the transfer of (*R*)-3-hydroxymyristic acid from its acyl carrier protein thioester to UDP-N-acetylglucosamine. LpxA is the first enzyme in the lipid A biosynthetic pathway and is a target for the design of antibiotics. The x-ray crystal structure of LpxA has been determined to 2.6 angstrom resolution and reveals a domain motif composed of parallel  $\beta$  strands, termed a left-handed parallel  $\beta$  helix ( $L\beta H$ ). This unusual fold displays repeated violations of the protein folding constraint requiring right-handed crossover connections between strands of parallel  $\beta$  sheets and may be present in other enzymes that share amino acid sequence homology to the repeated hexapeptide motif of LpxA.

The outermost membrane monolayer of Gram-negative bacteria is composed primarily of the lipid A moiety of lipopolysaccharide (LPS). The first step of lipid A biosynthesis in *Escherichia coli* is catalyzed by the cytosolic enzyme LpxA, which acts specifically to transfer the 14-carbon fatty acid, (*R*)-3-hydroxymyristate, from its acyl carrier protein thioester to the 3'-OH position of UDP-N-acetylglucosamine (1). LpxA and other enzymes of lipid A biosynthesis are essential for bacterial growth, as well as the maintenance of the permeability barrier function of the outer membrane (2).

The *lpxA* gene from *E. coli* has been cloned and encodes a subunit of 262 residues (3). The amino acid sequence is similar to that of several other enzymes, most of which are bacterial acetyl- and acyltransferases (4–6), including the enzyme that catalyzes the third step of lipid A biosynthesis, UDP-3-O-(*R*-3-hydroxymyristoyl)-glucosamine N-acyltransferase (LpxD; FirA) (7). The region

of sequence similarity common to all of these enzymes is a tandem-repeated imperfect six-residue sequence motif termed a "hexapeptide repeat" (6) or an "isoleucine patch" (5). This motif is characterized by an aliphatic residue at every sixth position (usually Ile, Val, or Leu) and a small residue (Ala, Ser, Cys, Val, Thr, or Asn) preceding the hydrophobic residue at position *i*-2. Glycine often occupies the position immediately after the aliphatic residue position. The hexapeptide repeat sequence motif occurs 28 times in LpxA within the NH<sub>2</sub>-terminal 186 residues.

The x-ray crystal structure of LpxA was solved by the method of isomorphous replacement with two heavy-atom derivatives and refined to a conventional R factor of 18.4% at 2.6 Å resolution (8, 9). Crystallographic statistics are presented in Table 1. The atomic model reveals that LpxA is a trimer composed of three identical subunits that are related by a crystallographic threefold rotation axis (Fig. 1). Each subunit is composed of two domains: an NH<sub>2</sub>-terminal domain of predominantly parallel  $\beta$ -sheet structure (residues 1 to 186) and a COOH-terminal domain (residues 187 to 262) containing four  $\alpha$  helices. The polypeptide

C. R. H. Raetz, Department of Biochemistry, Duke University Medical Center, Durham, NC 22710, USA.  
S. L. Roderick, Department of Biochemistry, Albert Einstein College of Medicine, Bronx, NY 10461, USA.

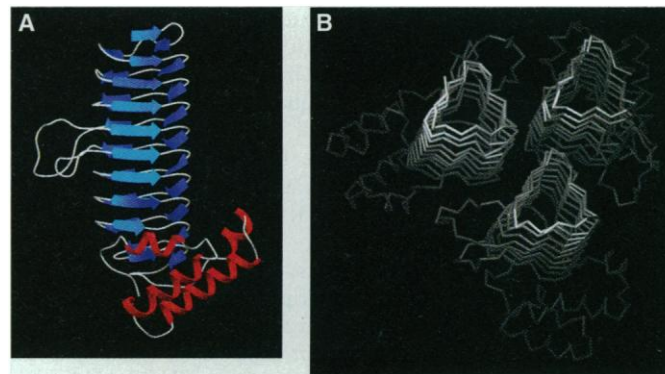
\*To whom correspondence should be addressed.

chain in the NH<sub>2</sub>-terminal domain, which contains tandem copies of the hexapeptide sequence motif, is coiled in a markedly regular left-handed triangular helix of 10 coils interrupted at two corners by external loops. The overall fold of this domain closely approximates an equilateral prism with dimensions of 17 by 39 Å. Its central axis is very nearly parallel to the crystallographic threefold axis that relates individual subunits of the trimer. We term this structural motif a left-handed parallel β helix (LβH) in order to emphasize the highly unusual left-handed crossover connections between the strands of its three parallel β sheets (see below) and its coiled conformation.

Six of the 10 helical coils of the LβH domain are uninterrupted, are composed of 18 residues (three hexapeptide units), and resemble equilateral triangles (Figs. 1B and 2). Of the remaining four coils, two are interrupted at corners by external loops. These polypeptide loops include residues 69 to 83 and 99 to 108, which disobey the hexapeptide repeat rule by the presence of the polar residues Asp<sup>74</sup> and Gln<sup>104</sup> at the aliphatic residue position required by the hexapeptide sequence motif. The first and last coils are abbreviated. Both the edges and corners of these triangular coils stack directly on top of adjacent coils and form interstrand hydrogen bonds to produce three flat, parallel β sheets that are the flat faces of the equilateral prism. The average separation distance of 4.8 Å between strands is typical for parallel β sheets.

The roles of the conserved residues of the hexapeptide repeat sequence motif are apparent from the crystal structure. For each 18-residue triangular coil, 6 side chains are directed inward, toward the axis of the prism, and 12 side chains point outward (Figs. 2 and 3). The six internal side chains of each turn are accounted for by the hydrophobic and small conserved positions of the hexapeptide repeat unit present in three copies for each coil. No charged residues are present in the interior of the LβH domain. Residues that occupy equivalent positions of adjacent helical coils stack directly on top of one another in regular ladders. The side chains of the conserved aliphatic residues point inward to form the hydrophobic core of the LβH domain. These residues, predominantly valine and isoleucine, adopt side-chain torsion angles that are staggered relative to the main chain and produce a cupped fit of these side chains with equivalent side chains of adjacent coils. This hydrophobic core packing scheme produces a long, narrow channel with a diameter of approximately 2 to 3 Å that is coincident with the helical axis. This channel is too narrow to accommodate solvent, and none is observed. The conserved small residues of the hexapeptide repeat

**Fig. 1.** (A) Ribbon diagram of a single subunit of LpxA. The NH<sub>2</sub>-terminus is positioned at the top of the diagram. The β strands of the left-handed parallel β helix (LβH) domain are indicated in blue as broadened arrows. The largely α-helical COOH-terminal domain is displayed in red at the bottom of the diagram. (B) α-Carbon trace of trimeric LpxA viewed nearly parallel to the crystallographic threefold rotation axis. Figures produced by SETOR (30).



motif also point inward and occupy positions immediately after each corner of a triangular coil. Small, polar residues at these positions (Cys, Thr, and Asn) hydrogen bond to main-chain and side-chain groups of adjacent coils and may stabilize the tight turn at each corner. Three asparagine residues, Asn<sup>60</sup>, Asn<sup>90</sup>, and Asn<sup>115</sup>, occupy equivalent positions in three consecutive coils. The side chains of these residues hydrogen bond to one another and to main-chain peptide groups of adjacent coils. Glycine is found in the position immediately after the aliphatic residue in 11 of 28 hexapeptide units. Other residue types at these positions would frequently produce unfavorably close contacts of their side-chain atoms with the carbonyl oxygen and side-chain atoms of residues in the tight turn of the succeeding coil.

The short β strands that form the faces of the LβH domain are usually composed of two residues (10). These strands are separated by hydrogen-bonded turns or non-bonded bends that redirect the main chain

by 120°. The main-chain torsion angles for these two residue bends are often similar to those of classical type II tight turns (11). The average main-chain torsion angles  $\phi$ ,  $\Psi$  for the first residue are  $-69^\circ$ ,  $143^\circ$ . The second residue frequently makes use of a nonglycine residue in left-handed  $\alpha$  conformation with average main-chain torsion angles  $\phi$ ,  $\Psi$  of  $63^\circ$ ,  $21^\circ$ . The central peptide plane of these turns is nearly perpendicular to the plane of the coil, allowing the amide nitrogen and carbonyl oxygen to hydrogen bond to peptide groups of tight turns in adjacent coils. The side chains of residues that project outward from one column of these tight turns and the residues that immediately flank these turns are responsible for forming the majority of interactions between subunits of the trimeric enzyme.

The last helical coil is abbreviated and leads to a COOH-terminal domain that lacks the characteristic hexapeptide repeat sequence motif. This domain contains four  $\alpha$  helices within the residue range 199 to 253. The location of the active site of LpxA

**Table 1.** Isomorphous replacement phasing statistics for LpxA with PHMPS (1 mM *p*-hydroxymercuriphenylsulfonic acid; 1-hour soak) and *cis*-Pt(NH<sub>3</sub>)<sub>2</sub>Cl<sub>2</sub> (1 mM; 2-hour soak) derivative crystals. The total number of observed reflections, the number of unique reflections, the completeness of the data, and the mean  $\langle I/\sigma(I) \rangle$  on the basis of counting statistics are given for the three data sets measured to 2.6 Å resolution. The refined relative occupancies, coordinates, and thermal factors are also tabulated. Overall figure of merit for 8605 reflections to 2.6 Å = 0.56.

Data	Observed	Unique	Completeness	$\langle I/\sigma(I) \rangle$	$R_{\text{merge}}^*$	$R_{\text{iso}}^\dagger$			
Native	79727	8860	0.87	23.7	0.063	—			
PHMPS	90691	8681	0.85	24.1	0.071	0.100			
<i>cis</i> -Pt(NH <sub>3</sub> ) <sub>2</sub> Cl <sub>2</sub>	91362	8641	0.85	17.6	0.092	0.089			
Data	Site	Occupancy	X	Y	Z	B	$f_c/\text{LOC}^\ddagger$	$R_c^\S$	
PHMPS	1	0.51	0.6945	0.6544	0.4506	19.1	1.82	0.63	
<i>cis</i> -Pt(NH <sub>3</sub> ) <sub>2</sub> Cl <sub>2</sub>	1	0.56	0.9059	0.9589	0.6313	31.4	1.41	0.63	
	2	0.37	0.4995	0.8027	0.6728	22.8			

\* $R_{\text{merge}} = \sum |I_i - \langle I \rangle| / \sum I_i$  within one data set.  $\dagger R_{\text{iso}} = \sum |F_{\text{Nat}} - F_{\text{Der}}| / \sum |F_{\text{Nat}}|$  between native and derivative data sets.  $\ddagger f_c/\text{LOC} = \text{rms heavy-atom structure factor amplitude} / \text{rms lack-of-closure}$ .  $\S R_c = \sum |f_{\text{H,obs}}| - |f_{\text{H,calc}}| / \sum |f_{\text{H,obs}}|$  for the 857 and 834 centric reflections measured for the two derivative crystals.

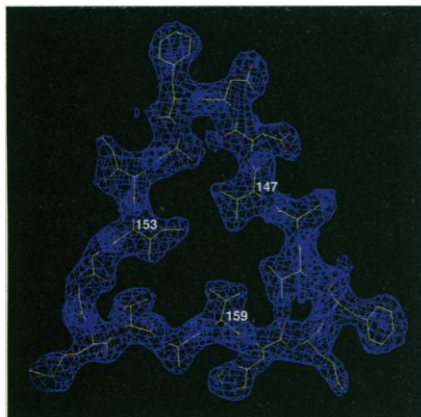


**Fig. 2.** Residues 145 to 162 of the LβH domain viewed parallel to the crystallographic threefold rotation axis. Electron density from the final  $2F_o - F_c$  map is also depicted. These residues correspond to those of coil C8 of Fig. 3. The  $\alpha$ -carbon atoms of three conserved aliphatic residues are labeled (Val<sup>147</sup>, Ile<sup>153</sup>, Val<sup>159</sup>).

and regions that bind its sugar nucleotide and acyl-acyl carrier protein substrates is not known (12). However, most of the enzymes that display the hexapeptide repeat sequence motif use acyl-coenzyme A or acyl-acyl carrier protein as substrates (2), both of which contain a characteristic phosphopantothienyl moiety. This may imply a contribution of the LβH domain toward binding of these structurally similar donors.

Since 1993, the crystal structures of several proteins that have domains composed entirely of parallel  $\beta$  structure have been determined (13). These proteins all fold as large, right-handed  $\beta$  coils with either two or three  $\beta$  strands per helical turn. Proteins with three strands per turn include the peptate lyases C (14) and E (15) from *Erwinia chrysanthemi* and from *Bacillus subtilis* (16), and the P22 tailspike protein (17). These proteins share some structural similarities with the LβH domain of LpxA, including an overall coiled fold and the flat, parallel  $\beta$

sheets that promote several different types of repetitive interactions between residues of adjacent coils. Interactions common to both right- and left-handed  $\beta$  helices include the hydrogen bonds between strands of the parallel  $\beta$  sheets, the cupped stacking of aliphatic residues, and the interactions of small polar residues near tight turns, such as the short column of three asparagine residues observed in LpxA that adopt interactions similar to those of the asparagine residues found in the "Asn ladders" of peptate lyases (15).

Despite these similarities, the LβH domain structure of LpxA reported here differs markedly from previously described protein structures. The fold of the LβH domain allows formation of a well-packed and nearly symmetric hydrophobic core in the context of a highly symmetric main-chain conformation promoted by tandem repeats of the hexapeptide sequence motif. The symmetry of the LβH fold is disrupted only minimally by the two polypeptide loops that project from the LβH domain. The abundance of extremely rare left-handed crossover connections between  $\beta$  strands of LpxA is in contrast to the nearly complete absence of such connections found in the protein structural database in preference to right-handed crossovers. This preference has been recognized since 1976 as a highly unusual and predictable long-range feature of protein supersecondary structure (18, 19) and has been attributed to a variety of factors. The inherent right-handed twist of extended polypeptide and  $\alpha$ -helical segments naturally folds into right-handed coils as the ends of these segments are brought together (18). In addition, the shorter and more compact right-handed crossover connections between strands of parallel sheets that are twisted in the common right-handed sense (20) are thought to be energetically more favorable (21), as are the packing interactions between  $\beta$

strands and right-handed crossover segments composed of  $\alpha$  helices (22). It may be significant that the latter two arguments favoring right-handedness would not apply to the LβH domain of LpxA, because the length of crossover connections between strands of its parallel  $\beta$  sheets, which are extremely flat and untwisted, would not favor either hand, and the crossover connections between strands are not composed of  $\alpha$  helices.

REFERENCES AND NOTES

1. M. S. Anderson and C. R. H. Raetz, *J. Biol. Chem.* **262**, 5159 (1987).
2. S. M. Galloway and C. R. H. Raetz, *ibid.* **265**, 6394 (1990); K. Young and L. L. Silver, *J. Bacteriol.* **173**, 3609 (1991); R. Vuorio and M. Vaara, *Antimicrob. Agents Chemother.* **36**, 826 (1992); R. Parent and P. H. Roy, *J. Bacteriol.* **174**, 2891 (1992); K. Young *et al.*, *Fed. Proc.* **7**, 1252 (1993); C. R. H. Raetz, *J. Bacteriol.* **175**, 5745 (1993); J. Allignet and N. El Solh, *Antimicrob. Agents Chemother.* **39**, 2027 (1995).
3. J. Coleman and C. R. H. Raetz, *J. Bacteriol.* **170**, 1268 (1988).
4. R. Vuorio, L. Hirvas, M. Vaara, *FEBS Lett.* **292**, 90 (1991).
5. I. B. Dicker and S. Seetharam, *Mol. Microbiol.* **6**, 817 (1992).
6. R. Vuorio, T. Harkonen, M. Tolvanen, M. Vaara, *FEBS Lett.* **337**, 289 (1994).
7. T. M. Kelly, S. A. Stachula, C. R. H. Raetz, M. S. Anderson, *J. Biol. Chem.* **268**, 19866 (1993).
8. We isolated LpxA from *E. coli* MC1061 cells harboring the plasmid pSR1, containing an arabinose-inducible promoter and the *lpxA* gene (12, 23). The purification scheme makes use of affinity, gel filtration, and ion-exchange chromatography. Single crystals suitable for x-ray diffraction analysis were prepared by the hanging drop vapor diffusion method from solutions of 1.9 M sodium phosphate-potassium phosphate containing 15 to 20% (v/v) dimethylsulfoxide (pH 6.2 to 6.8) (24). These crystals belong to the cubic space group P2<sub>1</sub>3 (*a* = 98.6 Å), contain 57% solvent, and diffract x-rays to 2.6 Å resolution. Data from mercury- and platinum-derivative crystals were measured with a Siemens X1000 area detector and reduced with the XDS program package (25). The program package PHASES (26) was used for isomorphous replacement phasing and solvent flattening. The high quality of the solvent-flattened map and the appearance of ordinary right-handed  $\alpha$  helices served to confirm the correct determination of chirality. This map supported an immediate and unambiguous trace of the polypeptide chain. Least-squares refinement of the atomic model of LpxA against x-ray diffraction and stereochemical observations was carried out by simulated annealing and conjugate direction procedures coded in the X-PLOR (27) and TNT (28) computer program packages. The current atomic model, lacking added solvent molecules, has been refined to a conventional crystallographic *R* factor of 18.4% at 2.6 Å resolution with all available x-ray diffraction data. The root-mean-square (rms) deviations of bond lengths and bond angles from ideal values are 0.012 Å and 2.4°, respectively. A Ramachandran plot of the main-chain torsion angles  $\phi$  and  $\psi$  shows just one residue in a disallowed conformation. The correctness of the atomic model of LpxA is also supported by the heavy-atom positions, which occupy sterically and chemically reasonable environments. The single mercury site binds near Cys<sup>163</sup>, and the two platinum-binding sites are found near Met<sup>1</sup> and His<sup>160</sup>. An additional minor platinum atom, located with phases of the refined model, binds between the side chains of His<sup>125</sup> and His<sup>144</sup>. The coordinates of LpxA have been deposited in the Brookhaven Protein Data Bank (1LXA).
9. During the course of atomic model building, it be-

**Fig. 3.** Structurally based amino acid alignment within the LβH domain of LpxA identifying equivalent residues of each coil. PB1, PB2, and PB3 denote the parallel  $\beta$  strands; T1, T2, and T3 denote turn residues according to the nomenclature of Yoder *et al.* (15). C1 to C10 identify individual coils of the helix.

	PB1	T1	PB2	T2	PB3	T3
C1	•		•		•	
C2	M I D	K S	A F V H	P T	A I V E	E G
C3	A S I G	A N	A H I G	P F	C I V G	P H
C4	V E I G	E G	T V L K	S H	V V V N	G H
C5	T K I G	R D	N E I Y	Q F	A S I	Loop 1
C6	V E I G	D R	N R I R	E S	V T I	Loop 2
C7	T K V G	S D	N L L M	I N	A H I A	H D
C8	C T V G	N R	C I L A	N N	A T L A	G H
C9	V S V D	D F	A I I G	G M	T A V H	Q F
C10	C I I G	A H	V M V G	G C	S G V	[ A Q ]
	--D V P	P Y	V I---	COOH-terminal domain		

The amino acid sequence for residues 1 to 186 of the LβH domain are arranged so that each row corresponds to a helical coil and each column to a single ladder of aligned residues in the three-dimensional structure. The residues of the conserved aliphatic residue position *i* referred to in the text are enclosed in boxes; residues of the conserved small residue position *i*-2 are arranged in columns marked by •. Single-letter abbreviations for the amino acid residues are as follows: A, Ala; C, Cys; D, Asp; E, Glu; F, Phe; G, Gly; H, His; I, Ile; K, Lys; L, Leu; M, Met; N, Asn; P, Pro; Q, Gln; R, Arg; S, Ser; T, Thr; V, Val; and Y, Tyr.

- came apparent that at least one residue, Val<sup>65</sup>, did not fit the electron density well in either solvent-flattened or model-phased  $2F_o - F_c$  maps. This observation and an inconsistent subunit mass determined by triple quadrupole electrospray mass spectrometry led us to resequence the plasmid DNA that had been used to overexpress LpxA. Discrepancies with the published DNA sequence corresponding to three altered amino acids were detected: Ser<sup>64</sup>→Gln, Val<sup>65</sup>→Phe, and Asp<sup>125</sup>→His (3). The new sequence is consistent with a derived subunit mass of 28,081 mass units, in agreement with the  $28,083 \pm 3$  mass unit value determined by mass spectrometry (29).
10. We define residues that participate in  $\beta$  strands as those with main-chain  $\phi$ ,  $\psi$  angles that are characteristic of ordinary  $\beta$  structures and that form interstrand hydrogen bonds with backbone amide and carbonyl groups.
  11. J. S. Richardson, *Adv. Protein Chem.* **34**, 167 (1981).
  12. M. S. Anderson et al., *J. Biol. Chem.* **268**, 19858 (1993).
  13. M. D. Yoder and F. Jumak, *FASEB J.* **9**, 335 (1995).
  14. M. D. Yoder, N. T. Keen, F. Jumak, *Science* **260**, 1503 (1993).
  15. M. D. Yoder, S. E. Lietzke, F. Jumak, *Structure* **1**, 241 (1993).
  16. R. Pickersgill, J. Jenkins, G. Harris, W. Nasser, J. Robert-Baudouy, *Nature Struct. Biol.* **1**, 717 (1994).
  17. S. Steinbacher et al., *Science* **265**, 383 (1994).
  18. J. S. Richardson, *Proc. Natl. Acad. Sci. U.S.A.* **73**, 2619 (1976).
  19. K. Nagano, *J. Mol. Biol.* **109**, 235 (1977).
  20. C. Chothia, *ibid.* **75**, 295 (1973).
  21. M. J. E. Sternberg and J. M. Thornton, *ibid.* **110**, 269 (1977).
  22. K.-C. Chou, G. Nemethy, M. Pottle, H. A. Scheraga, *ibid.* **205**, 241 (1987).
  23. D. N. Crowell, M. S. Anderson, C. R. H. Raetz, *J. Bacteriol.* **168**, 152 (1986).
  24. U. Pfltzner, C. R. H. Raetz, S. L. Roderick, *Proteins Struct. Funct. Genet.* **22**, 191 (1995).
  25. W. Kabsch, *J. Appl. Crystallogr.* **21**, 916 (1988).

26. W. Furey and S. Swaminathan, *American Crystallographic Association Meeting Summaries (abstr.)*, **73** (1995).
27. A. T. Brunger, A. Krukowski, J. W. Erickson, *Acta Crystallogr.* **A46**, 585 (1990).
28. D. E. Tronrud, L. F. Ten Eyck, B. W. Matthews, *ibid.* **A43**, 489 (1987).
29. C. R. H. Raetz and S. L. Roderick, data not shown.
30. S. V. Evans, *J. Mol. Graphics* **11**, 134 (1993).
31. We gratefully acknowledge U. Pfltzner for technical assistance, R. Zheng for aid in DNA sequencing work, X.-J. Tang of the Albert Einstein College of Medicine Laboratory for Macromolecular Analysis for mass spectrometry, and M. Anderson, J. Blanchard, M. Degano, and G. Scapin for many helpful discussions. Supported in part by National Institutes of Health grants GM51310 (to C.R.H.R.) and AI38328 (to S.L.R.).

30 August 1995; accepted 12 October 1995

## Elementary Computation of Object Approach by a Wide-Field Visual Neuron

Nicholas Hatsopoulos,\* Fabrizio Gabbiani, Gilles Laurent†

An essential function of the brain is to detect threats, such as those posed by objects or predators on a collision course. A wide-field, movement-sensitive visual neuron in the brain of the locust was studied by presenting simulated approaching, receding, and translating objects. The neuron's responses could be described simply by multiplying the velocity of the image edge ( $d\theta/dt$ ) with an exponential function of the size of the object's image on the retina ( $e^{-\alpha\theta}$ ). Because this product peaks before the image reaches its maximum size during approach, this neuron can anticipate collision. The neuron's activity peaks approximately when the approaching object reaches a certain angular size. Because this neuron receives distinct inputs about image size and velocity, the dendritic tree of a single neuron may function as a biophysical device that can carry out a multiplication of two independent input signals.

Vision plays an important role in notifying animals of imminent danger, such as an impending collision with a predator or an environmental surface. One possible strategy for collision avoidance is for the animal to react when the object is at a given distance away from it. This would require that the animal estimate depth, using cues such as motion or binocular parallax. Many animals, such as arthropods, can avoid rapidly approaching objects, but are unlikely to use this strategy because their binocular fields and the spacing between their eyes are too small.

A second possible strategy is to react at a given time before collision by monitoring the symmetrical expansion of the image projected on the retina by the approaching object (1). Behavioral and electrophysiological evidence from birds and flies support the use of this strategy (2). Imagine an object subtending an angle  $\theta$  at a distance  $d$  from the eye (Fig. 1A). If this object moves toward

the animal at a constant velocity  $v$ , its image on the retina will grow increasingly faster as the object approaches ( $\dot{\theta}$  will increase nonlinearly as  $\theta$  increases; the dot means time derivative). The tau function (3),

$$\tau(t) = \frac{d}{\dot{d}} = \frac{\sin\theta \cos\theta}{\dot{\theta}} \approx \frac{\theta}{\dot{\theta}} \text{ if } \theta \text{ small}$$

where  $t$  is time, is useful because it can provide the time before collision without any explicit knowledge of  $d$ . The tau function can be obtained from the optical flow field and requires only knowledge of  $\theta$  and  $\dot{\theta}$ , which can both be determined monocularly at the retina. The function  $\tau(t)$  (4) could be encoded in the firing rate of a neuron, and an escape command would be triggered when  $\tau(t)$  has decreased to below a threshold value (Fig. 1C). Alternatively, the brain could compute  $1/\tau(t)$ , which peaks at collision (Fig. 1C). In this case, an escape command would be triggered when  $1/\tau(t)$  exceeds a certain threshold. In either case, the timing of escape depends on determining that a threshold has been crossed, which is a difficult problem for biological systems. We now report that a pair of identified neurons

in an insect brain adopts yet a different strategy to track object approach, combining  $\theta$  and  $\dot{\theta}$  nonlinearly to yield a response profile similar to the function  $f(t)$  (Fig. 1C).

We studied the LGMD and DCMD neurons (Fig. 1B), two connected, motion-sensitive neurons in the brain of the locust *Schistocerca americana* (5–7). These visual neurons respond to novel, small contrasting object motion, regardless of direction or orientation, and are inhibited by large-field motion (such as flow fields generated by the animal's own motion) (8). More recent investigations (9, 10) have shown that the LGMD and DCMD neurons respond preferentially to approaching rather than translating objects and have suggested that the feature most closely correlated with their firing is angular acceleration of the image edges (11).

We recorded the response of DCMD to simulated "approaching" objects presented monocularly to the animal (12) and noted that it differs significantly from the acceleration profile of the image. First, when a simulated object approached the animal at low but constant velocity (a condition in which image angular velocity and acceleration increase as the image grows larger), DCMD activity peaked before the image acceleration was maximal (Fig. 2A) (13). If DCMD tracked image acceleration, its firing rate should not decrease before the acceleration peak (14). The timing of the DCMD peak firing rate was strongly correlated with the collision time (Fig. 2C, regression coefficient = 0.963,  $r^2 = 0.9998$ ) (15). The delay between peak firing and collision, however, was a function of both object size and object velocity (Fig. 2D). This indicates that DCMD does not encode  $\tau(t)$  [or  $1/\tau(t)$ ], because  $\tau$  is independent of these two parameters. Second, when the simulated object decelerated while approaching the animal (image angular velocity held constant, that is, image acceleration  $\dot{\theta} = 0$ ), DCMD responded strongly at first and continued firing, although progressively less strongly, as the simulated object

California Institute of Technology, Biology Division, Pasadena, CA 91125, USA.

\*Present address: Department of Neuroscience, Brown University, Providence, RI 02912, USA.

†To whom correspondence should be addressed. E-mail: laurentg@stabase1.caltech.edu